The Thermodynamic Transformation of the Tropical Subcloud Layer by Precipitation and Downdrafts

ALAN K. BETTS

Department of Atmospheric Science, Colorado State University, Fort Collins, Colo. 80523

(Manuscript received 9 September 1975, in revised form 27 January 1976)

ABSTRACT

The transformation by precipitation of the well-mixed subcloud layer into a new structure which is nearly wet adiabatic and has a lower moist static energy is presented. A simple two-layer model is used to show that the precipitating convection appears to strip off the subcloud layer which ascends in updrafts, and to replace it with an equal layer of air from just above cloud base, which descends in downdrafts associated with the evaporation of falling rain. The mean transformation is presented, and the incorporation of the results into a parametric model of the transformation of the subcloud layer is discussed.

1. Introduction

An important unresolved problem in tropical meteorology is the transformation of the boundary layer by convective rain. In the past few years, mixed layer models have been proposed and incorporated into large-scale tropical numerical models (e.g., Deardorff, 1972; Betts, 1973a; Arakawa and Schubert, 1974). However, it is known that the well-mixed subcloud layer which prevails in undisturbed conditions is transformed by precipitating disturbances into a different, more stable structure (Garstang and Betts, 1974; Echternacht and Garstang, 1975). Moist downdrafts play an important role in this transformation. The purpose of this paper is to analyze this transformation using tropical data over Venezuela, and develop a simple parametric model.

Models for the undisturbed well-mixed subcloud layer have supposed (e.g., Betts, 1973a) that air rising to form cumulus clouds has the mixed layer properties while the environment between clouds subsides in compensation and is rapidly incorporated into the more turbulent subcloud layer, which preserves a reasonably homogeneous structure. This is clearly a simplification—acoustic radar studies (e.g., Frisch and Clifford, 1974) have shown considerable variations in time in the depth of the mixed layer. With the onset of precipitation, two new processes increase the coupling between cloud and subcloud layers, and transform the mixed layer structure. Evaporation of falling precipitation into the unsaturated subcloud layer is a heat sink and a source of water vapor, bringing the layer closer to saturation at constant equivalent potential temperature. In addition, evaporative cooling can drive convective-scale downdrafts with a mass transport comparable to the convective updrafts. This downward transport brings down air which was initially potentially warmer and drier than the air in the subcloud layer. These two processes oppose each other in the sense that evaporation cools and moistens while downward transport warms and dries. Any combination can therefore result. Typically, in the cases examined here, the subcloud layer becomes cooler and drier after the precipitation and downdrafts, indicating the need to consider both processes.

These processes have been known for a long time (Byers and Braham, 1949; Riehl and Malkus, 1958; Ludlam, 1963). Zipser (1969) showed the extent of the influence of the downdraft circulation in his analysis of a Pacific disturbance. More recently, Gray (1973) has emphasized the importance of calculating the large magnitudes of both up and down cloud-scale circulations, and Betts (1973b) attempted to estimate their magnitudes from a composite budget study. However, a boundary layer model which incorporates moist cloud-scale updrafts and moist downdrafts associated with the evaporation of precipitation has been lacking. This paper, one of several which analyze different aspects of the convection over Venezuela, will attempt to develop such a model based on observations.

CONCEPTUAL MODEL

The observations suggest a simple two-layer structure in which the subcloud layer (in front of the mesosystem) rises in updrafts and is replaced by air from the layer immediately above, which descends with the evaporation of precipitation in moist downdrafts. Theoretical support for this model is given in Moncrieff and Miller (1976). They developed analytical and nu-

merical models for the squall line type of convection and discussed their updraft-downdraft structure. They concluded from a three-dimensional numerical simulation of one of the Venezuelan squall lines that the downdraft originates at low levels from the layer immediately overlying the updraft air. They present a model structure similar to that shown in Figs. 1 and 2. Their squall line case is included in this data set (storm 47 in Table 1). Indeed it appears that some aspects of their models for the squall line type of convective transfer may have a wider applicability since not all the convective systems in the data set presented here could be described as travelling squall lines. Some were quite small mesosystems (rain area $\sim$400 km^2) which passed over the observation site. All, however, were characterized by low-level relative inflow in the front (from the west).

Fig. 1 shows schematically the model used in this paper for a moving mesosystem embedded in a larger scale flow. It is characteristic of those over Venezuela. In front of the system at low levels there is a region of inflow and behind it a modified area. This modified air is assumed to come from the spreading out of downdraft air.

In the first part of the paper (Sections 2–5) observational models are discussed for this *local* transformation. Single rawinsonde soundings will be taken as representative of the air before and after the passage of the mesosystem over the rawinsonde site. Necessarily this involves the assumption that the inflow and outflow regions are homogeneous. Typically, the inflow and first outflow soundings were about 50 min (equivalent to 30 km at 10 m s^{-1}) away from the passage of the rain area over the site. Later soundings in the outflow region (typically $\sim$140 min after the rain) naturally showed some variability (Table 1) but, in general, the outflow structure persisted for some hours into the night (when no further rawinsondes were launched). Typically, the rain systems passed over the observation site in late afternoon or early evening. In these observational models, only the change in structure is considered, *not* the mass fluxes associated with inflow and outflow. These *fluxes* could be associated in Fig. 1 with the rate of change of inflow and outflow areas. The mass fluxes associated with inflow and outflow or updraft and downdraft (which are clearly important to the effect of the mesosystem on the large-scale flow) are treated separately in this paper in Section 6.

This separation into one model for the change of structure and one for the associated mass fluxes for inflow and outflow does depend on the assumption of homogeneity of structure in the inflow and outflow regions. For a parametric model it seems a necessary simplification.

The observational models (Sections 2–5) relate the outflow structure after the system (subscript A in Fig. 1) to the inflow structure before (subscript B). The parametric model of Section 6b places this model in the context of grid-averaged variables and mass fluxes.

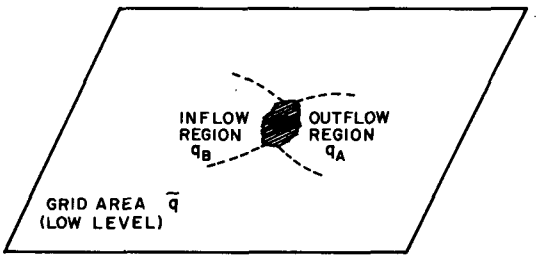

FIG. 1. Schematic large-scale grid area for a low-level pressure surface showing embedded moving mesoscale rain system (shaded). Dotted inflow and modified outflow regions are shown: subscript B denotes before system and A after it, while q is the specific humidity.

2. The experiment

The data were collected during the second Venezuelan International Meteorological and Hydrological Experiment (VIMHEX 1972) which was conducted in north-central Venezuela during the summer of 1972. A major objective of the experiment was the study of tropical convection, particularly organized cumulonimbus systems, with the view toward developing parametric models of the type presented here. The summer rainy season is characterized on disturbed days by traveling mesoscale convective systems ranging from large squall lines (instantaneous rain area $\sim$2000 km^2) to smaller systems (rain area $\sim$few hundred km^2). Typically, about a third to a half of the days had significant rainfall associated with these mesosystems.

The experimental design was very simple. A 10 cm calibrated weather radar (an extensively modified M-33) and a GMD-1 rawinsonde system were placed at Carrizal, Venezuela (9°22.8′N, 66°55.0′W) within a raingage network of diameter 120 km. Sequential soundings were launched (every 65–90 min) whenever significant radar activity was observed. Rainfall and radar echo statistics are available in Betts and Stevens (1974). The region is relatively flat and uniform, and the dominant echo motion was from east to west at 7–15 m s^{-1} with low-level relative inflow into systems from the west. Thus, in general, a line section of soundings were obtained depicting the atmospheric structure in front of, inside, and then behind a raining convective system which passed over the observation site. Typically, the preceding sounding showed an undisturbed atmospheric structure with a well-defined nearly mixed layer up to cloud base, while after the passage of a system, the sounding showed a dramatically different atmospheric structure with a cooling of the lower layer and a fall of equivalent potential temperature θ_e or moist static energy h.

Although the rain systems seen on radar varied widely in size, top height, travel speed and apparent organization, the thermodynamic boundary layer transformations which they produced on passing over the observation site were remarkably similar. In this paper, therefore, no distinction has been made between types of storm systems, and the results are considered common to all the summer's storms. It should be noted, however, that one rain event (of the night of 1–2 September; see Table 1) was much larger in time and space scale than any of the others. The radar echo area reached a maximum area of 10^4 km^2, and lasted about 12 h. It is included in this set despite its synoptic-scale character because the total transformation of the lower atmosphere still fitted the models presented in Sections 3, 4 and 5.

The dynamic transformation of the boundary layer for a subset of these storms will be discussed in another paper. A further paper (Betts *et al.*, 1976) compares the travel speeds for some of the mesosystems discussed in this paper with the predictions of the analytic squall line model proposed by Moncrieff and Miller (1976).

The rawinsonde used was the VIZ 1290 series sonde with a modified humidity duct (Friedman, 1972), which appears to have overcome the large humidity errors of earlier sondes (Betts *et al.*, 1974). Temperature and relative humidity were computed from strip-chart values at every baroswitch contact point (where the sonde switches from the temperature to humidity sensor). In low levels, baroswitch contact points are spaced at known pressure intervals of ~10 mb. Humidity values are missing every five contact points where a reference signal is sampled: these were interpolated linearly from adjacent values. The thermodynamic data thus have a vertical resolution of about 10 mb. To facilitate averaging of soundings, and to use the model presented in Section 3, data were derived for standard 10 mb levels by interpolating between adjacent contact point levels.

Balloons were inflated to a constant lift giving an ascent rate which averaged 4.8 m s^{-1} at low levels.

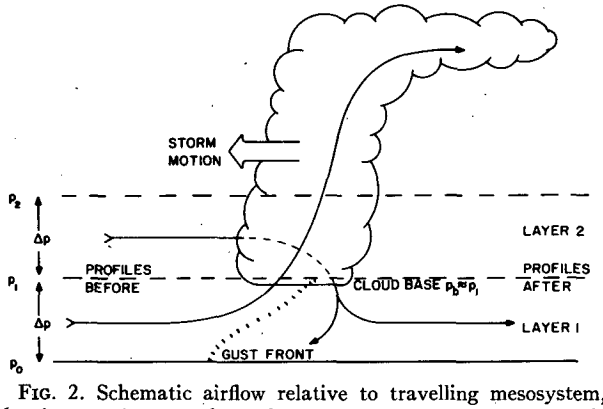

FIG. 2. Schematic airflow relative to travelling mesosystem, showing two-layer model exchange: inflow layer p_0 to p_1 ascends in updrafts and inflow layer p_1 to p_2 descends in downdrafts in replacement. (Actual flow inside system will be both three-dimensional and transient, not two-dimensional as sketched.)

Thus, 10 mb in the vertical at low levels corresponds to about 20 s. The time constants of the thermistor and hygristor are not well known. Brousaides and Morrissey (1974) give theoretical and observed thermal response times of 15 and 19 s, respectively, for the carbon strip hygristor used in this sonde for similar ascent rates. The thermistor time constant is considerably smaller, about 5 s, but not well documented. Betts *et al.* (1974), who neglected the thermistor lag time, estimated the differential lag of thermistor and hygristor (which determines errors in the mixing ratio) to be rather smaller—about 6 s. In this paper no lag corrections have been made. If thermistor and hygristor time constants are taken as 5 and 15 s, respectively, the systematic temperature and mixing ratio errors would be (for a dry adiabatic layer)

$$\left.\begin{aligned}\delta T &\approx +0.25 \text{ K}\\ \delta q &\approx -0.4 \text{ g kg}^{-1}\end{aligned}\right\}.$$

Together, these systematic errors mean that the uncorrected data will *overestimate* the lifting condensation level height by about 85 m (9 mb). The *lowest* LCL heights (highest pressures) in the subcloud layer preceding the rain system will be used as estimates of cloud base to help offset this error (see Section 3c).

The lifting condensation level, hydrostatic height z, and many derived parameters (static energies and potential temperatures) were computed for each data level. Collectively, these parameters were used to examine the low-level structure. For the purposes of this paper, we shall use primarily static energies since these are additive functions. The static energy s is defined as

$$s = C_p T + gz, \tag{1a}$$

the moist static energy as

$$h = s + Lq, \tag{1b}$$

where q is the specific humidity, and the saturation static energy as

$$h_s = s + Lq_s, \tag{1c}$$

where q_s is the saturation specific humidity.

3. Simple model for the local transformation

The passage of a rain system in general produced a marked low-level cooling, stabilization, and fall of moist static energy h (and equivalent potential temperature θ_e). The evaporation of falling rain into the subcloud layer would produce a cooling and stabilization, but at constant h or θ_e as discussed in Section 1. We assume that a mass transport process, presumably in downdrafts from higher in the atmosphere, produces the observed fall of h or θ_e; and develop a simple mass transport model for this transformation to interpret the data and derive certain characteristic parameters.

The model is presented in Fig. 2. The convective system removes a surface layer thickness $\Delta p = p_0 - p_1$,

which ascends in updrafts, and replaces it by the layer above (from p_1 to p_2 where $\Delta p = p_1 - p_2$) which descends in downdrafts. The model thus relates a spacial or temporal change in the surface layer to the structure of the undisturbed atmosphere preceding the convective system. Fig. 2 is schematic: we shall not consider the detailed kinematics of the exchange at all. The crucial concept here is that given an initially horizontally homogeneous atmosphere with a typical stratification of θ_e or h (which we shall *assume* is that given by the preceding undisturbed atmosphere) then a low-level fall of θ_e or h can only result from a vertical exchange, updrafts taking up high θ_e air and downdrafts bringing down low θ_e air. We have chosen the very simplest exchange involving only two layers, so that we can relate the surface layer (p_0 to p_1) structure after a rain system to that of the undisturbed atmosphere before the system; p_1 is determined independently of cloud base p_b by the model but the two are found to be close (see Section 3c).

a. Evidence for downdraft from just above cloud base

A specific example of a vertical cross section through the gust front of the downdraft just as it reached the observation site is shown in Fig. 3. Sounding 226 was made an hour prior to the arrival of a squall line system (storm number 60); sounding 227 was successfully launched just after the arrival of the cool surface gust but before the heavy precipitation; and 228 was after the system rain area had passed. The ascent through the gust front shows a layer of cool, low h downdraft air 35 mb thick with a sharp upper boundary at 950 mb. This air has a moist static energy corresponding to the air at or just above cloud base in soundings 226 and 227, indicating that the air in the downdraft gust came from just above cloud base. The wind values show a low-level gust [these values are 2 min average winds (about 60 mb) interpolated to 25 mb intervals]. Sounding 228, 80 min later, shows the deep layer of cooled, low h air, which is typical of the transformations listed in Table 1.

Moncrieff and Miller (1976) simulated the development of storm 47 (see Table 1) which also had a squall line structure. They perturbed a three-dimensional primitive equation model initialized with sounding 176 which proceeded the arrival of the squall lines. The model developed a quasi-steady, propagating squall line type structure which travelled with the leading edge of a cold pool of air, itself in turn maintained by downdrafts from individual cumulonimbus cells. The model showed that the downdrafts originated from low levels from the layer immediately overlying the updraft air. The authors also computed the transformation of the atmosphere produced by the model convective system and found qualitative agreement with the changes observed.

In an earlier paper, Betts (1973b) concluded from a composite cumulonimbus budget study over Venezuela that air descended typically only 80 mb in downdrafts, although descending air appeared to exist up to 500 mb in the decaying stage of systems. Those results involved considerable averaging: this study suggests (see Section 3c) that at low levels downdraft air descends approximately the depth of the subcloud layer ($\sim$130 mb). Zipser (1969) and many mid-latitude studies have concluded that downdraft air originates in the middle troposphere or at least as high as 600 mb. This is a rather deeper downdraft than those studied here, where p_2 in Fig. 1 was only about 650 mb in the deeper cases. An analysis of mid-latitude data, where

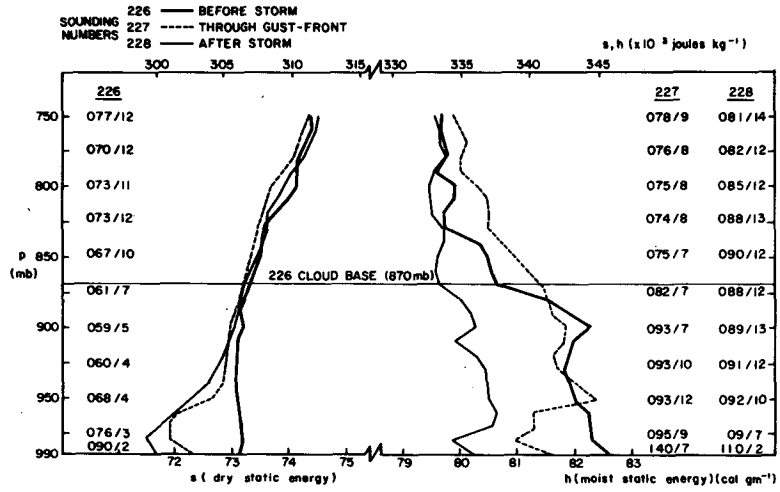

FIG. 3. Cross section through a squall line. Sounding 226 (1759 local time) is well in front, 227 (1907 local time) ascended through the gust-front, and 228 (2028 local time) was after the passage of the system. Wind velocities (in degrees and m s^{-1}) at 25 mb intervals are shown.

cloud bases are often higher, using this two-layer model would be useful.

b. Diagnostic solution

The model represented by Fig. 2 is solved diagnostically to find the value of Δp which will produce the observed "after" mean h in the layer p_0 to p_1.

Formally, we define layer-average values of moist static energy h, and find Δp such that

$$\bar{h}_{2B}=\frac{1}{\Delta p}\int_{p_2}^{p_1} h_B dp=\bar{h}_{1A}=\frac{1}{\Delta p}\int_{p_1}^{p_0} h_A dp, \quad (2)$$

where $p_0-p_1=p_2-p_1=\Delta p$. Subscript B is used to denote a value before the system passage and subscript A afterward. The surface layer p_0 to p_1 (after the system) has descended from the layer p_1 to p_2 (before the system) with conservation of layer mean h (see Fig. 1). One can then calculate the mean evaporation of liquid water necessary to produce this descent. Since $\bar{h}_{2B}=\bar{h}_{1A}$ and $h=s+Lq$, then this mean evaporation of liquid water, which we shall denote $\bar{E}$ (in energy units), is given by

$$\begin{aligned}\bar{E}&=\overline{Lq}_{1A}-\overline{Lq}_{2B}\\&=\bar{s}_{2B}-\bar{s}_{1A},\end{aligned} \quad (3)$$

where the averages have the same meaning as in Eq. (2). That is, although $\bar{h}$ is conserved in the descent, $\bar{s}$ decreases through evaporation of liquid water and $\overline{Lq}$ increases the same amount. It should be noted, however, that these changes of $\bar{s}$ and $\overline{Lq}$ are *not* the changes that have occurred with the passage of the rain system in the lower layer p_0 to p_1. These changes ($\bar{s}_{1A}-\bar{s}_{1B}$, $\overline{Lq}_{1A}-\overline{Lq}_{1B}$) are quite different because before the system the upper layer (2B) is warmer and drier than the lower layer (1B). This model actually partitions the change $\bar{s}_{1A}-\bar{s}_{1B}$ into two components: one due to the initial stratification $\bar{s}_{2B}-\bar{s}_{1B}$ and one due to evaporation $\bar{E}$.

Thus, the application of this simple model to the observed low-level change produces two basic parameters, Δp and $\bar{E}$. It might be useful to contrast this model with the mixed subcloud-layer model proposed in Betts (1973a). In that model, air rose from the subcloud layer to form clouds and the environment subsided slowly and dry adiabatically between the clouds. A cloud mass flux ω^* was defined to parameterize this exchange. In this model, once again air rises from the lower layer p_0 to p_1 [which we find (Section 3c) appears to correspond very well with the subcloud layer], but it is replaced in a discrete exchange by air from above, which descends with evaporation of liquid water. Thus, a new parameter for this evaporation is introduced. The parameter Δp, however, could still be related to a cloud base mass flux (see Section 6c), with the introduction of a time scale.

In the next section, we derive $\bar{E}$ and Δp and compare Δp with the depth of the subcloud layer before the rain system.

c. Derivation of model parameters Δp, $\bar{E}$

The radar echo information was examined for the whole experiment to find those occasions when storm systems passed over the observation site. The rawinsonde time series were examined in relation to the echo position to select those soundings which were before and those after the storm passage. In some cases, there were two or more soundings after the storm passage (see Table 1). Occasionally, two storms passed between the before-after pair of soundings. These before-after sounding pairs were tabulated, and run through a program to determine Δp using Eq. (2). Δp was increased in steps of 10 mb until $\Delta\bar{h}=\bar{h}_{2B}-\bar{h}_{1A}$ changed sign. This gave Δp to ± 5 mb, corresponding to the smallest value of $\Delta\bar{h}$. Using this Δp, $\bar{E}$ was computed using Eq. (3).

The derived layer thickness Δp was compared with the thickness of the subcloud layer p_0-p_b preceding the rain system. Cloud base pressure p_b was estimated from lifting condensation levels (LCL) in the well-mixed layer preceding the storm. Lifting condensation level pressures (LCLP) were computed for the mixed layer data levels of the sounding before the storm system. The typical variation of these LCLP in the mixed layer is ± 10 mb, with a maximum value of LCLP (corresponding to the lowest *height*) just above the superadiabatic layer (data levels 950–970 mb). Earlier studies with the VIMHEX data (Betts *et al.*, 1974) have shown good agreement between cloud base pressure and this extreme value of LCLP. Hence, this extreme value of LCLP was used here as an estimate of p_b. In some cases the surface layer of the before sounding showed shallow surface cooling from an earlier shower, and p_b was taken as the value of LCLP at the base of the mixed layer just above. These cloud base estimates (p_b) are presented in Table 1 together with the date, storm number, sounding numbers and the level $p_1=p_0-\Delta p$, as well as $\bar{E}$ given by Eq. (3). The surface pressure p_0 varied only slightly from 990 mb.

Fig. 4a shows a plot of Δp against the estimated cloud base for the before sounding in the before-after pair. The correlation is good with 18 out of 24 pairs lying within ± 20 mb (dashed lines) of a one to one agreement. The mean value of p_b-p_1 is 4 ± 17 mb with the three circled points excluded as lying beyond the 3σ limits. These three sounding pairs have been removed from the subsequent analysis, leaving 21 pairs.

Thus, the two-layer model corresponds very closely to the subcloud layer and an equal pressure depth layer above cloud base. In this model dealing with layer averages the travelling storm strips off the subcloud

TABLE 1. Storm parameters.

Date	Storm No.	Sounding Nos. Before	Sounding Nos. After	p_b mb	p_1 $(p_0-\Delta p)$ mb	$\bar{E}$ Eq. (3) J kg$^{-1}\times 10^3$
19 June	3	59	60	905	900	4.1
		59	61	905	910	4.1
27 June	12, 14	81	82	830	820	6.7
		81	83	830	810	6.0
3 July	27	100	101	865	870	5.7
		100	102	865	840	6.7
8 July	33	116	117	880	880	4.6
9 July	35	120	121	865	840	7.8
		120	122	865*	950*	4.3* (1)
		120	123	865	880	4.6
11 July	120	131	132	900	910	2.3
		131	133	900	890	3.5
24 July	47	176	177	830	820	9.5
		176	178	830*	910*	5.4* (1)
28 July	53	192	193	880	860	5.6
		192	194	880	900	4.1
31 July	56	203	204	825	840	7.4
7 August	60	226	228	870	890	4.9 (2)
11 August	64	241	242	840	820	6.8
		241	243	840	820	8.1
1–2 September	108, 109	312	317	830	830	8.8 (3)
		312	318	830	800	9.2
4 September	112	324	325	870*	820*	8.9* (1)
		324	326	870	890	2.5
		Average (excluding starred values)		862	858	5.9
Number of events	13					
Number of sounding pairs	24					

(1) Starred values fall outside 3σ limits on Fig. 4a and are excluded from averages.
(2) Sounding number 227 was launched into gust front (see Fig. 3).
(3) Major disturbance: soundings 313 to 316 were launched inside rain area.

layer which ascends in updrafts, and this layer is replaced by air from an equal pressure layer above cloud base which descends in downdrafts.

Fig. 4b shows a plot of $\bar{E}$ against Δp. As the layer thickness Δp increases, so does $\bar{E}$, the mean evaporation of liquid water into the downdraft. This is related to the fact that as Δp increases, the downdraft air has to descend a greater distance in a moist (though unsaturated) process from an initially higher level in the atmosphere. The evaporation is correspondingly greater. The dotted line has been drawn through the origin and the mean value of $\bar{E}$ for the sample, giving

$$\bar{E}=\epsilon\Delta p. \tag{4}$$

The slope ϵ is 4.5×10^3 J kg^{-1} (100 mb)$^{-1}$ [corresponding to an evaporation of 1.8 g kg^{-1} (100 mb)$^{-1}$]. There is clearly some scatter but for a model this is a convenient first approximation for $\bar{E}$. For this sample, the average value of Δp of 132 mb corresponds to a mean evaporation of liquid water of 2.4 g kg^{-1} in driving the downdraft into the subcloud layer. This is a relatively small fraction of the inflow subcloud layer $\bar{q}_{1B}\approx 15$ g kg^{-1} which, ignoring kinematic considerations, may be regarded as the water vapor available for condensation. However, we note that the total evaporation in the subcloud layer increases with Δp^2, i.e.,

$$\bar{E}\Delta p/L=\epsilon\Delta p^2/L,$$

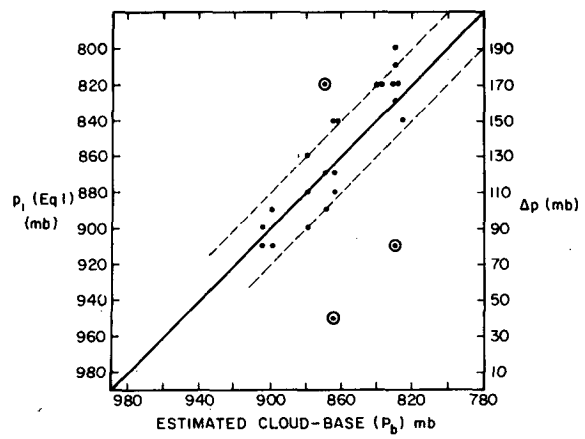

FIG. 4a. Plot of depth $\Delta p = p_0 - p_1$ of layer 1 (Fig. 2) given by the simple two-layer model of Eq. (2) as a function of cloud base estimated from subcloud layer lifting condensation levels before the arrival of a storm. Solid line is the one-to-one line; the dashed lines are drawn at ±20 mb. The circled points were omitted from the subsequent analysis.

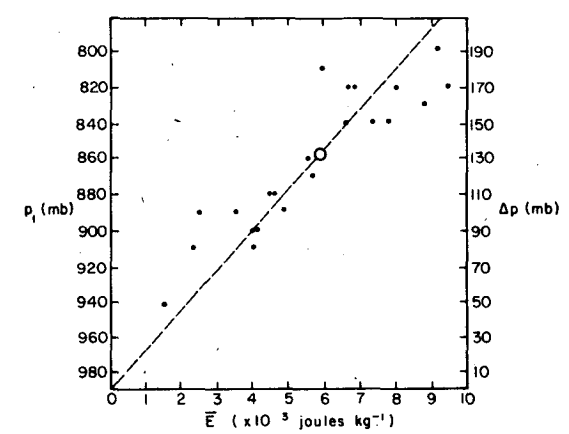

FIG. 4b. Plot of mean evaporation ($\bar{E}$) into descending downdraft air as a function of depth Δp of each layer in the simple two-layer model (Fig. 2). Dashed line is drawn through the origin and the sample mean value for $\bar{E}$ (denoted by open circle).

so that if the layer deepens, even with $\bar{q}_{1B}$ constant, then the ratio of the evaporation to available condensation ($\bar{q}_{1B}\Delta p$) increases.

4. Mean profiles before and after storm system passage

Section 3 presented the average evaporation associated with the low-level transformation. However, although $\bar{h}_{2B} = \bar{h}_{1A}$ in Eq. (2), the before and after profiles of h (and correspondingly s and q) could well differ. Fig. 5 presents the average before and after profiles of s, h, h_s and Lq, for the pairs in Table 1, excluding the three extreme cases which fall outside the 3σ limits of $p_b - p_1$. These averages were generated by a specific technique designed to preserve the two model layers. The sounding pressures were transformed to a coordinate

$$\hat{p} = \frac{p_0 - p}{\Delta p}$$

before interpolating the data to intervals of 0.05 in $\hat{p}$ from 0 to 2.0, and then averaging the 21 before soundings and the corresponding 21 after soundings. In Fig. 5 the pressure values corresponding to the surface $\hat{p}=0$ is 990 mb and to $\hat{p}=1$ is 858 mb (average value of p_1). Corresponding averages were also produced by scaling by $p_0 - p_b$ (corresponding to the subcloud layer) but they are essentially indistinguishable because of the close correlation of p_b and p_1 (Fig. 4a). These average profile changes necessarily satisfy Eq. (2) so that the lower layer (p_0 to p_1 or p_b) after the storm passage has a mean moist static energy equal to the mean static energy in the layer above cloud base preceding the storm. However, although $\bar{h}_{2B} = \bar{h}_{1A}$, Fig. 5 also shows a more well mixed h structure in the lower layer afterward than in the corresponding upper layer before. More remarkably, the mean temperature profile afterward shows saturation static energy h_s almost constant. This means that although the layer is not saturated, the temperature structure is nearly wet adiabatic. The relative humidity throughout most of the layer is about 76%, increasing to near 88% at the surface. An explanation for the well-mixed h_s structure is not obvious.

One feature still visible in this average profile after the downdrafts is an h_s minimum just above the surface with a more stable layer $0.1 < \hat{p} < 0.4$. Eight out of thirteen cases showed a low-level inversion or more stable layer of this type. This feature has been noticed by others (Hamilton and Archbold, 1945; Riehl and Lückefedt, 1973; Zipser, personal communication). Some of the after soundings showed no such inversion. When this feature occurs, and whether it is significant for grid-averaged models, needs further study. The model presented in the next section interprets in more detail the change of the *mean* vertical structure from the before to after profiles, by inferring a vertical profile for the evaporation into the layer, and also a parameter representing a degree of mixing within the layer.

Fig. 5 shows that thermally there is little change in s or h_s above cloud base—the dominant effect is from a dry to a near-wet adiabatic structure below cloud base. A simple parametric model formulating this change will be discussed in Section 6a. For moist static energy, the fall extends above cloud base to near $\hat{p} \approx 1.8$, where cross-over in the profiles occurs. Above this level, the typical increase in h after the rain is observed. The fall in h between $1.0 < \hat{p} < 1.8$ indicates downdrafts from above terminating in this layer. We shall not, however, extend the model in this paper to consider layers higher in the atmosphere.

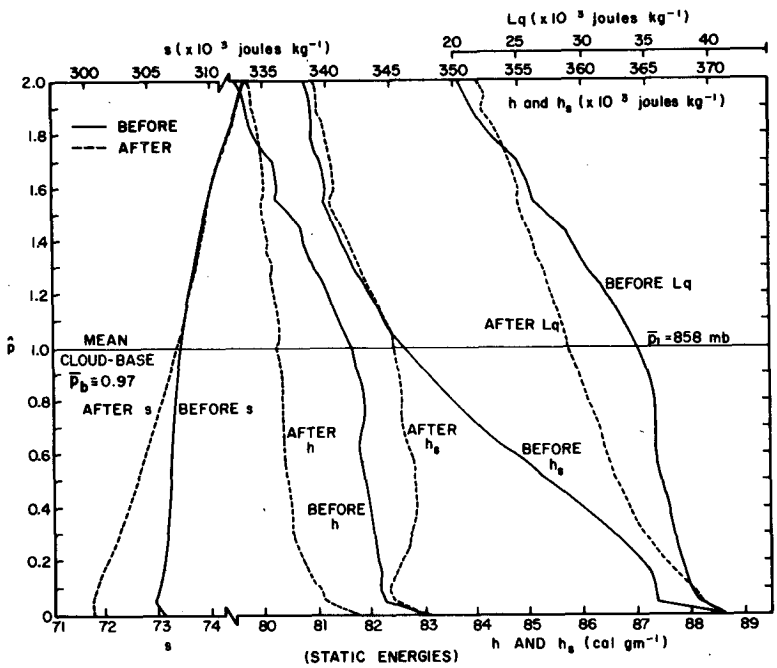

FIG. 5. Mean profiles before and after the passage of a convective system. The curves are averages of 21 before-after sounding pairs.

5. Diagnostic model with profile of evaporation and mixing

In Section 3, mean values of the evaporation $\bar{E}$ were computed to transform layer 2B to 1A. However, this does not completely specify the transformation, even if the before and after h profiles are identical $[h_A(p)=h_B(p-\Delta p)]$ unless the vertical profile of E is specified. In this case, however, it is straightforward to compute a profile $E(p)$ by differencing level by level $s_A(p)-s_B(p-\Delta p)$. If $h_A(p)\neq h_B(p-\Delta p)$, one could infer some mixing of the layer has taken place. A more well mixed h profile afterward will give a pattern of $h_A(p)-h_B(p-\Delta p)$ values which are negative below and then positive above. This is observed in 16 cases out of 21 and in the average (see Figs. 5 and 6). The diagnostic interpretation of this change requires some assumption.

We can represent the change between any pair of levels p_A and $(p-\Delta p)_B$ in the form

$$h_A=h_B+M_h, \tag{5a}$$

$$s_A=s_B-E+M_s, \tag{5b}$$

$$Lq_A=Lq_B+E+M_{Lq}. \tag{5c}$$

Only if the mixing terms, denoted M, are zero can one compute E. Otherwise, we have two independent equations [e.g., (5b) and (5c)] and three unknowns (E,M_s,M_{Lq}). Eq. (5a) is the sum of (5b) and (5c). A reasonable assumption is to relate the M terms to the deviation of the properties of the air at that level from the layer mean before the rain system. We shall suppose

$$M_s=-\alpha s'_B, \tag{6a}$$

$$M_{Lq}=-\alpha Lq'_B, \tag{6b}$$

where

$$s'_B=s_B-\bar{s}_{2B},$$

$$Lq'_B=L(q_B-\bar{q}_{2B}).$$

That is, the mixing is constrained to change s and Lq in a proportion α to their deviations from the layer mean before the passage of the rain system. Conceptually, this simple model says that if we consider inflow air, say with specific humidity q_B, entering the rain system at level p_B, only a fraction $(1-\alpha)$ follows the streamline from p_B to $p_A=p_B+\Delta p$. The remaining fraction α is removed (to enter a mixing process) and replaced by the same fraction α with the mean layer properties $\bar{q}_{2B}$. In addition, there is an evaporation E from falling rain. The outflow then results from a combination of three terms, i.e.,

$$q_A=(1-\alpha)q_B+\alpha\bar{q}_B+E,$$

which is Eq. (5c) using (6b). As defined, α will be positive, if M is a change toward the well-mixed state, represented by the layer mean. The value $\alpha=0$ corresponds to descent along streamlines without mixing and $\alpha=1$ corresponds to a layer well mixed in h afterward (as will be shown later, however, this does not necessarily apply to s). This model for mixing within the descending downdraft layer is self-consistent only if the mixing terms vanish when integrated over the

layer, that is, if

$$\int M_h = \int M_s = \int M_{Lq} = 0, \tag{7}$$

where the integration is over the whole layer which descends. $\int M_h$ is always zero from Eqs. (5a) and (2); $\int M_s$ and $\int M_{Lq}$ are zero for constant α (a useful simple case) but are not necessarily zero for arbitrary α.

As a diagnostic model, one can solve level by level for E and α. Substituting Eqs. (6a) and (6b) in Eqs. (5b) and (5c), one obtains for each level, the pair of equations

$$\begin{pmatrix} 1 & s'_B \\ -1 & Lq'_B \end{pmatrix}\begin{pmatrix} E \\ \alpha \end{pmatrix} = \begin{pmatrix} s_B - s_A \\ Lq_B - Lq_A \end{pmatrix}. \tag{8}$$

Solutions exist provided $h'_B = s'_B + Lq'_B \neq 0$. They are

$$E = [Lq'_B(s_B - s_A) - s'_B(Lq_B - Lq_A)]/h'_B, \tag{9a}$$

$$\alpha = (h_B - h_A)/h'_B. \tag{9b}$$

In the case (for a pair of levels) where $h_A = h_B$, $\alpha = 0$ from Eq. (9b), and from Eq. (1b)

$$s_B - s_A = Lq_A - Lq_B;$$

thus Eq. (9a) reduces to $E = Lq_A - Lq_B$ for each level pair. In general, we can interpret the observed level-by-level paired differences of s and Lq in terms of a profile of E and α.

Fig. 6 shows $h_A - h_B$, $s_B - s_A$, $Lq_A - Lq_B$, E and α for the averaged atmospheric change (Fig. 5). The method for finding α, E diverges in the middle of the layer where h'_B becomes small, so the values at $\hat{p} = 0.5$ have been omitted. A smooth trend of E is found, with the highest evaporation at the base of the layer; α is more variable but has a mean value of $+0.62$. Despite the variability of α, Eq. (7) is satisfied

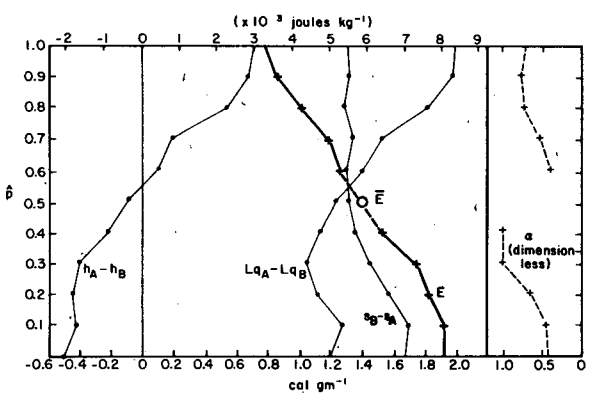

FIG. 6. The thin lines are the average vertical profiles of the before-after differences (from Fig. 5) between corresponding levels p and $p - \Delta p$ of moist static energy, dry static energy, and water vapor (as Lq) plotted against nondimensional pressure $\hat{p}$. The heavy line is the derived profile of the evaporation $E(\hat{p})$ and the heavy circle marks $\bar{E}$. The derived mixing parameter α (nondimensional) is shown on the right (dashed).

($\int M_s$, $\int M_{Lq} \lesssim 10^2$ J kg^{-1}) and the model is self-consistent. This seems to be a consequence of the fact that $h_B - h_A$, h'_B, s'_B and Lq'_B which comprise M_s and M_{Lq} [Eqs. (6)] are all approximately antisymmetric functions about the middle of the layer. The mean value of α of 0.62 indicates how well mixed in h the layer is afterward as mentioned above. If a constant value of $\alpha = 0.62$ were chosen, then the two curves of E calculated from Eqs. (5b) and (5c) differ from each other and from that found by solving Eqs. (8) by less than 10^3 J kg^{-1}. This suggests a constant α could be used for predictive purposes.

Fig. 5 is simply a breakdown of the observed mean change. It involves the further assumption on mixing [Eqs. (6)] but the results seem reasonable. For example, the negative values of $h_A - h_B$ near the surface after the rain indicate that some of this air must have come not from just above cloud base but from still higher in the atmosphere. The evaporation E into this air is highest, corresponding to the fact that this air, which has the largest negative $h_A - h_B$, has in some average sense descended the greatest distance. Nearer to cloud base after the rain, the reverse is true. Thus, this refined model indicates that some of the air near the surface after the rain has descended rather more than the depth of the subcloud layer, and some of the air higher in the layer rather less. Although the layer after the rain system has a more well mixed h structure than the upper layer before the system, despite the mixing, it has a *more stable* s structure, because the gradient of evaporation outweighs the mixing.

6. Parameterization of subcloud-layer transports

Sections 2–5 have discussed two diagnostic models for the observed local subcloud-layer transformation, but not the kinematics of the change (how much mass ascends in updrafts or descends in downdrafts) nor the difference which is related to the net mass convergence on the cloud scale. These questions of mass flux cannot be determined reliably from these data which are two-dimensional cross sections through travelling storms. Nonetheless, the cloud-scale mass fluxes (as was mentioned in Section 1) do determine the domain in time and space affected by the transformation, which is fundamental to constructing a parametric model for the process. Section 6b therefore reformulates the first model proposed in this paper into flux form and considers briefly the relation of the low-level transformation to larger scale dynamic parameters. Initially, in Section 6a, we summarize the observational conclusions about the *local* transformation and indicate the possibility of a slightly different model for some parametric purposes.

a. Local transformation

Section 3 presented a simple layer model for the change in the mean subcloud layer produced by the

passage of a mesosystem. The initial subcloud layer before the system is simply replaced by the descent of a layer initially above cloud base modified by the evaporation of liquid water given by Eq. (4).

Sections 4 and 5 examined and modelled the change in vertical structure associated with this transformation. A vertical profile of evaporation $E(p)$ and of a mixing parameter were derived for the data presented here (Figs. 5 and 6). A more well mixed h structure is observed after the downdrafts and rain than in the upper layer before. A parametric model for this change in vertical structure could use a simple linear profile of $E(p)$ and a constant value of α.

Another possible model (attractive because it is simple) suggested by Fig. 5 is to say that the structure of the lower layer afterward is well mixed in h and h_s. This is a lapse-rate adjustment approach. As before, $\bar{h}_{1A}=\bar{h}_{2B}$. The $\bar{h}_{s1A}$ value could be calculated from the $\bar{s}$ profile in the upper layer before the rain and the mean evaporation given by Eq. (4). However, Fig. 5 (and a study of the individual before-after profile pairs) suggest that $\bar{h}_{s1A}$ is quite close to h_{sB} at cloud base. The temperature change is essentially from dry to wet adiabatic with the layer of cooling *confined to the subcloud layer*. If we denote $\Gamma_B=-(\partial s/\partial p)_B$ for the layer $1<\hat{p}<2$ and $\Gamma_w=-(\partial s/\partial p)$ for the wet adiabat, then, if we take Γ_B, Γ_w as constant as in Fig. 7, the difference in s between corresponding levels is given by a linear relationship

$$s_B(p-\Delta p)-s_A(p)=\Gamma_B(p_0-p)+\Gamma_w(p-p_B). \quad (10)$$

This is a useful parametric formulation because it expresses the change in terms of lapse rates: one observed, and one calculated. In addition, Eq. (10) implicitly specifies the evaporation associated with the change. Averaged over the layer, Eq. (10) gives

$$\bar{E}=\bar{s}_{2B}-\bar{s}_{1A}=\tfrac{1}{2}(\Gamma_B+\Gamma_w)\Delta p=\epsilon'\Delta p. \quad (11)$$

Substituting values for Γ_B and Γ_w gives $\epsilon'=4.7.10^3$ J kg^{-1} (100 mb)$^{-1}$ which differs only slightly from ϵ in Eq. (4). Thus, Eq. (10) is a satisfactory approximation to the observations and it could be used in a parametric model instead of Eq. (4). This lapse rate adjustment approach implicitly implies both $\alpha=1$, because h_A is well mixed and a specific profile of $E(p)$. From Eqs. (10), (5b) and (6a) or Fig. 7, we find

$$E(p)=\tfrac{1}{2}\Gamma_B\Delta p+\Gamma_w(p-p_B). \quad (12)$$

Thus E increases from 2.6×10^3 J kg^{-1} at cloud base to 9.8×10^3 J kg^{-1} at the surface; this is a slightly greater average than shown in Fig. 6, since a larger mixing parameter ($\alpha=1$) has been assumed.

Fig. 7 illustrates this idealized model showing the distinct, well-mixed layers before and after the rain. The change in h above cloud base has not been discussed, but simplifying Fig. 5, we have let the h change go linearly to zero at $p=2$. Note that the lifting condensation level of the initial idealized well-mixed layer

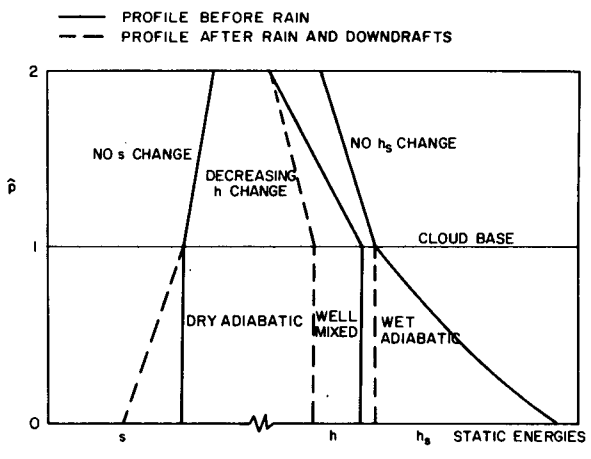

FIG. 7. Idealized model showing well-mixed dry adiabatic structure before convective rain and downdrafts and well-mixed wet adiabatic but unsaturated structure afterward.

is a little above the cloud base shown. Unfortunately, a theoretical basis for the structure after precipitation, a well-mixed, wet adiabatic but unsaturated layer, is lacking in sharp contrast to the well-mixed dry adiabatic layer before the arrival of the rain system. The relative humidity and lapse rate in the downdraft air could depend not only on the convective dynamics but also on the microphysics, since the downdrafts are driven by droplet evaporation. It is not clear how a nearly well-mixed wet adiabatic structure can be achieved in downdraft air which is never saturated. As mentioned in Section 4, some (but not all) of the after profiles showed low-level inversions which have been considerably smoothed by the averaging in Fig. 5, indicating a more complex multi-level process. However, for parametric purposes, the simpler models presented here with two layers, or an essentially linear variation of evaporation may be adequate. Clearly, however, the characteristic structures of the low-level atmosphere after precipitation and downdrafts need further study.

b. Flux formulation of the transformation

In this section, we formulate the local transformation in flux form for inclusion in large-scale averaged equations. The conceptual model was presented in Figs. 1 and 2. For simplicity, we consider just the entire subcloud layer and reformulate the subcloud-layer transformation in terms of a flux through cloud base. Following Yanai *et al.* (1973) we consider a moist static energy equation, averaged over a large-scale grid area (the average being denoted by terms with a tilde):

$$\frac{\partial\tilde{h}}{\partial t}+\tilde{\mathbf{v}}\cdot\nabla\tilde{h}+\frac{\partial}{\partial p}\tilde{\omega}\tilde{h}=-\frac{\partial}{\partial p}(\widetilde{\omega' h'})+Q_R. \quad (13)$$

Horizontal eddy transports have been neglected, and Q_R is a radiative source term. Formally, if we integrate

this equation over the subcloud layer we shall require $F_{h0}=\widetilde{\omega' h_0'}$ at the surface and $F_{hb}=\widetilde{\omega' h_b'}$ at cloud base. The specification of the surface flux (which would clearly be complicated especially over the ocean) will not be discussed. We suppose that the cloud base flux results only from the updraft and down draft circulations modelled in Section 3, and a distinct vertical environmental mass flux remote from the mesoscale system. With simple definitions for mean parameters, $\widetilde{\omega' h_b'}$ can then be expressed in terms of the model proposed in this paper. By definition, the convective eddy flux of h at cloud base F_{hb} is

$$F_{hb}=\widetilde{\omega' h_b'}=\widetilde{\omega h}_b-\tilde{\omega}_b\tilde{h}_b. \tag{14}$$

Suppose we now define averaged updraft, downdraft and environmental mass fluxes at cloud base:

$$\left.\begin{aligned}\omega_u^*&=\frac{1}{A}\int\omega_u dA_u\\ \omega_d^*&=\frac{1}{A}\int\omega_d dA_d\\ \omega_e^*&=\frac{1}{A}\int\omega_e dA_e\end{aligned}\right\}, \tag{15}$$

where A_u, A_d, A_e are the areas of updraft, downdraft and environment and A $(=A_u+A_d+A_e)$ is a large-scale grid area. The large-scale mean vertical motion $\tilde{\omega}_b$ is given by

$$\tilde{\omega}_b=\omega_e^*+\omega_u^*+\omega_d^*. \tag{16}$$

We now make some simplifications. First, in the schematic model of Fig. 2, we suppose that we can associate layer-mean values $\bar{h}_{1B}$ and $\bar{h}_{1A}$ with the updraft and downdraft mass fluxes ω_u^* and ω_d^* as they pass through cloud base. This assumes uniform layers of mass inflow and outflow. Further, we define the environmental cloud base h flux as $\omega_e^* h_{eb}$ where h_{eb} is an environmental horizontal average. This assumes that either h_{eb} or ω_e are horizontally uniform. Then $\widetilde{\omega h}_b$ in Eq. (14) expands as

$$\widetilde{\omega h}_b=\omega_e^* h_{eb}+\omega_u^*\bar{h}_{1B}+\omega_d^*\bar{h}_{1A}. \tag{17}$$

Clearly further simplification of Eq. (14) depends on the definition of mean fields: How do h_e and $\tilde{h}$ relate to the before and after values of h discussed in Sections 3 and 4? This is a crucial definition which determines $\widetilde{\omega' h_b'}$ in Eq. (14). The simplest assumption which we shall make is to take the before condition, the environment, and the large-scale average as all approximately the same: that is

$$\tilde{h}\approx h_e\approx h_B. \tag{18}$$

This requires that the area covered by the downdraft from the rain system be small compared with the grid area, as well as the assumption that the inflow h_B to the rain system can be approximated by a large-scale average. The advantage of approximation [Eq. (18)] is that it avoids the specification of the areas affected by the rain system, but it may be unsatisfactory for some convective regimes. For example, the inflow air might be moister than the large-scale average.

Substituting Eqs. (16)–(18) at cloud base in Eq. (14) and using $\bar{h}_{1A}=\bar{h}_{2B}$ [Eq. (2)] gives

$$F_{hb}=\omega_u^*(\bar{h}_{1B}-h_{Bb})+\omega_d^*(\bar{h}_{2B}-h_{Bb}), \tag{19}$$

where $h_{Bb}(=\tilde{h}_b)$ denotes a cloud base value before the rain system. We have chosen to write Eq. (19) in terms of h_B variables rather than $\tilde{h}$, for comparison with the earlier models of this paper. The two terms in Eq. (19) are self-explanatory. The first represents the effect of the updraft in removing air with mean properties $\bar{h}_{1B}$ through cloud base where the moist static energy has the value h_{Bb}. This term will be small to the extent that the subcloud layer before the rain system is well mixed up to cloud base. The second term is the effect of the intrusion of downdraft air into the subcloud layer and this will typically be the dominant term. Equation (19) contains only moist static energies of the atmosphere before the rain system, which we have supposed equal to a large-scale average state. Rearranging Eq. (19) gives

$$F_{hb}=(\omega_u^*+\omega_d^*)(\bar{h}_{1B}-h_{Bb})+\omega_d^*(\bar{h}_{2B}-\bar{h}_{1B}). \tag{20}$$

Now, the first term will also be small [compare Eq. (19)] to the extent that updraft and downdraft mass fluxes partly cancel, while the second is the replacement of updraft air by downdraft air. $\omega_u^*+\omega_d^*$ is a measure of the net mass transport by the convective system through cloud base. Clearly, the relationship between updraft mass fluxes is a crucial undetermined parameter. We define a "mesoscale structure parameter" β such that

$$\left.\begin{aligned}\omega_u^*&=\beta(\omega_u^*+\omega_d^*)\\ \omega_d^*&=(1-\beta)(\omega_u^*+\omega_d^*)\end{aligned}\right\}. \tag{21}$$

Typically, $\beta>1$: Gray (1973) has suggested that $\beta\approx 2$ and Betts (1973b, Fig. 6) gave a rough estimate of β at cloud base of 2.5. Given β, which may well vary for different convective regimes, we have now specified the cloud base convective h flux in terms of the net convective mass transport $(\omega_u^*+\omega_d^*)$ through cloud base. However, the relationship of $\omega_u^*+\omega_d^*$ to the large-scale mean field $\tilde{\omega}$ remains unresolved since ω_e^* is a further independent parameter.[1]

Using Eq. (21) we have the final expression

$$F_{hb}=(\omega_u^*+\omega_d^*)[(\bar{h}_{1B}-h_{Bb})+(1-\beta)(\bar{h}_{2B}-\bar{h}_{1B})]. \tag{22a}$$

[1] The model used in Sections 3, 5 and Fig. 2 neglects ω_e between the before and after rawinsondes.

In the large-scale static energy and water budget equations, the corresponding fluxes are the coupled fluxes of static energy and liquid water $F_s - F_{Ll}$ and total water $F_{Lq} + F_{Ll}$ (in energy units; l denotes liquid water) [see Betts (1975)]. However, the model of Section 3 gives the evaporation $\bar{E}$ of liquid water, which is the flux difference ΔF_{Ll} across the subcloud layer. We have not computed the surface fluxes F_{s0} or F_{q0}, or the surface rainfall. The equations corresponding to Eq. (22a) are

$$F_{sb} - \Delta F_{Ll} = (\omega_u^* + \omega_d^*)[(\bar{s}_{1B} - s_{Bb}) + (1-\beta)(\bar{s}_{2B} - \bar{s}_{1B} - \bar{E})], \quad (22b)$$

$$F_{Lqb} + \Delta F_{Ll} = (\omega_u^* + \omega_d^*)[(L\bar{q}_{1B} - Lq_{Bb}) + (1-\beta)(L\bar{q}_{2B} - L\bar{q}_{1B} + \bar{E})], \quad (22c)$$

with $\bar{E}$ given by (4) or (11) depending on the model used. Equations (22) have been developed for the mean subcloud layer. For incorporation into large-scale averaged equations, the surface fluxes are also needed, as well as some relationship between $(\omega_u^* + \omega_d^*)$ and large-scale mean parameters such as $\tilde{\omega}$. If a more detailed structure of the subcloud layer is needed, then the models of Sections 5 or 6a could be expressed in flux form.

c. Relation of Δp to ω_d^*

The parameter Δp introduced in Section 3 can be used to replace ω_d^* using the expression

$$\omega_d^* A = \Delta p \frac{d\mathcal{A}}{dt}, \quad (23)$$

where $d\mathcal{A}/dt$, the rate of spreading of the downdraft air, is assumed independent of pressure below cloud base. Equations (21) and (23) then relate the divergence of the downdraft to the net horizontal divergence in the subcloud layer associated with the mesosystem which we denote $\overline{\nabla \cdot \mathbf{V}}^*$ (averaged with respect to pressure and scaled to the grid area A), i.e.,

$$\frac{1}{A}\frac{d\mathcal{A}}{dt} = (1-\beta)\frac{\omega_u^* + \omega_d^*}{\Delta p} = (1-\beta)\overline{\nabla \cdot \mathbf{V}}^*.$$

Thus, a horizontal divergence is the time scale which relates Δp to a vertical mass flux.

7. Summary and conclusions

This paper has examined diagnostically the thermodynamic transformation of the subcloud layer associated with convection over Venezuela. The characteristic nearly-well-mixed, dry-adiabatic layer preceding a rain system is transformed by downdrafts and evaporating precipitation to a new structure after the system passage. This new structure is thermally cooler with a nearly-wet-adiabatic structure, but unsaturated with a lower moist static energy (and θ_e) than the atmosphere preceding the rain. The moist static energy profile is also not far from being well-mixed. A simple two-layer model shows that the convective system appears to strip off the subcloud layer (to ascend in updrafts) and replaces it by an equal layer of air just above cloud base. This layer descends in downdrafts associated with the evaporation of falling rain. The mean evaporation involved in this downdraft circulation was calculated and shown to increase with the depth of the subcloud layer.

The low-level origin of the downdraft has been confirmed independently by Moncrieff and Miller (1976) who present a numerical simulation of the development of one of the squall lines contained in this data set.

By averaging 21 pairs of soundings, the mean before and after profiles for the transformation were presented. These were used to derive a vertical profile of the evaporation and of a mixing parameter using a more detailed model which involved a proportionality assumption on mixing. The vertical structure of moist static energy in the subcloud layer after the rain system passage was more well-mixed than in the corresponding layer above cloud base before the rain. Although this seems reasonable in a turbulent overturning process, it is unclear how a nearly-wet-adiabatic thermal structure is achieved in downdraft air which is never saturated. A simple parametric model was proposed (Fig. 7) for the local subcloud transformation involving the replacement of the preceding nearly-dry-adiabatic structure by a wet-adiabatic structure while conserving the mean moist static energy of the layer above.

In Section 6b, the subcloud transformation was re-expressed in flux form suitable for inclusion in large-scale averaged equations. However, many questions associated with the detailed kinematics and dynamics of the updraft and downdraft circulations remain unresolved. This paper simply expressed them as an as yet unknown "mesoscale structure" parameter. In addition, this paper does not attempt a closed parameterization theory, which requires the development of relationships between the net cloud-scale transports (e.g., $\omega_u^* + \omega_d^*$) and the large-scale mean parameters such as $\tilde{\omega}$.

Acknowledgments. This research was supported by the National Science Foundation, Global Atmospheric Research Program, under Grant OCD72-01406, and both the National Science Foundation and the GATE Project Office, NOAA, under Grant OCD74-21678. The VIMHEX 1972 field experiment was also supported by the Office of Naval Research under Contract N0014-68A-0493-002 (Principal Investigator: Dr. H. Riehl), the Meteorological Service of the Venezuelan Air Force, and the Facilities Laboratory of the National Center for Atmospheric Research. R. Miller was responsible for the data processing and computing,

P. Martin for further data reduction, and S. Kuehl for typing the manuscript.

I am also grateful for the research cooperation of Drs. M. W. Moncrieff and M. J. Miller of the Atmospheric Physics Group, Imperial College, London.

REFERENCES

Arakawa, A., and W. Schubert, 1974: Interaction of a cumulus cloud ensemble with the large-scale environment. Part I. *J. Atmos. Sci.*, **31**, 674–701.

Betts, A. K., 1973a: Non-precipitating cumulus convection and its parameterization. *Quart. J. Roy. Meteor. Soc.*, **99**, 178–196.

——, 1973b: A composite mesoscale cumulonimbus budget. *J. Atmos. Sci.*, **30**, 597–610.

——, 1975: Parametric interpretation of trade wind cumulus budget studies. *J. Atmos. Sci.*, **32**, 1934–1945.

——, and M. A. Stevens, 1974: Rainfall and radar echo statistics: VIMHEX 1972 research report, 151 pp. [Available from the Department of Atmospheric Science, Colorado State University].

——, F. J. Dugan and R. W. Grover, 1974: Residual errors of the VIZ radiosonde hygristor as deduced from observations of subcloud layer structure. *Bull. Amer. Meteor. Soc.*, **55**, 1123–1125.

——, R. W. Grover and M. W. Moncrieff, 1976: Structure and motion of tropical squall lines over Venezuela. *Quart. J. Roy. Meteor. Soc.*, **102** (in press).

Brousaides, F. J., and J. F. Morrissey, 1974: Residual temperature-induced humidity errors in the National Weather Service radiosonde. AFCRL Report TR-74-0111, L. G. Hanscom Field, Bedford, Mass.

Byers, H. R., and R. R. Braham, 1949: *The Thunderstorm.* Washington, D. C., Govt. Printing Office, 287 pp.

Deardorff, J. W., 1972: Parameterization of the planetary boundary layer for use in general circulation models. *Mon. Wea. Rev.*, **100**, 93–106.

Echternacht, K. L., and M. Garstang, 1975: Changes in the structure of the tropical subcloud layer from the undisturbed to disturbed states. Submitted to *Mon. Wea. Rev.*

Friedman, M., 1972: A new radiosonde case: The problem and the solution. *Bull. Amer. Meteor. Soc.*, **53**, 884–887.

Frisch, A. S., and S. F. Clifford, 1974: A study of convection capped by a stable layer using Doppler radar and acoustic echo sounders. *J. Atmos. Sci.*, **31**, 1622–1628.

Garstang, M., and A. K. Betts, 1974: A review of the tropical boundary layer and cumulus convection: Structure, parameterization and modelling. *Bull. Amer. Meteor. Soc.*, **55**, 1195–1205.

Gray, W. M., 1973: Cumulus convection and larger scale circulations: I. Broadscale and mesoscale considerations. *Mon. Wea. Rev.*, **101**, 839–855.

Hamilton, R. A., and J. W. Archbold, 1945: Meteorology of Nigeria and adjacent territory. *Quart. J. Roy. Meteor. Soc.*, **71**, 231–262.

Ludlam, F. H., 1963: Severe local storms: A review. *Meteor. Monogr.*, No. 27, 1–30.

Moncrieff, M. W., and M. J. Miller, 1976: The dynamics and simulation of tropical cumulonimbus and squall lines. *Quart. J. Roy. Meteor. Soc.*, **102** (in press).

Riehl, H., and J. S. Malkus, 1958: On the heat balance in the equatorial trough zone. *Geophysica*, **6**, 503–538.

——, and W. Lückefedt, 1973: Tropical convective cloud masses and atmospheric circulation. *Beitr. Berliner Wetterkarte*, No. 96, 1–15.

Yanai, M., S. Esbensen and J. Chu, 1973: Determination of the bulk properties of tropical cloud clusters from large-scale heat and moisture budgets. *J. Atmos. Sci.*, **30**, 611–627.

Zipser, E. J., 1969: The role of organized unsaturated convective downdrafts in the structure and decay of an equatorial disturbance. *J. Appl. Meteor.*, **8**, 799–814.